Noise-reduced electroless deposition of arrays of copper filaments

Yu-Yan Weng, Jian-Wen Si, Wen-Ting Gao, Zhe Wu, Mu Wang,* Ru-Wen Peng, and Nai-Ben Ming
National Laboratory of Solid State Microstructures and Department of Physics, Nanjing University, Nanjing 210093, China
(Received 9 October 2005; revised manuscript received 19 December 2005; published 1 May 2006)

We report here a self-organized electroless deposition of copper in an ultrathin layer of $CuSO_4$ electrolyte. Microscopically the branching rate of the copper deposits is significantly decreased, forming an array of smooth polycrystalline filaments. Compared with a conventional electrodeposition system, no macroscopic electric field is involved and the thickness of the electrolyte layer is greatly decreased. Therefore the electroless deposition takes place in a nearly ideal, two-dimensional diffusion-limited environment. We suggest that restriction of the thickness of the electrolyte film is responsible for the generation of smoother branches of the electrodeposits. Our data also show that even in a diffusion-limited scenario the aggregate morphology is not necessarily very ramified and fractal-like.

DOI: 10.1103/PhysRevE.73.051601 PACS number(s): 81.15.Pq, 45.70.Qj, 68.43.Jk, 82.80.Fk

I. INTRODUCTION

Pattern formation and pattern selection have been interesting topics in far-from-equilibrium interfacial growth for decades [1–8]. Among many systems, electrodeposition has attracted much attention [9–16] because of the rich variation of growth morphologies in the system and the simplicity of the experimental setup. By changing experimental conditions, the metal deposits may vary from dendrite [17–21] to dense branching morphology [22–24], fractals [12,25–30], fingering [31,32], and even network patterns [33]. It is generally believed that macroscopically the electrodeposition process can be described by a mass transport equation in an electric field [34]. In some cases people tried to ignore the effects of convection and electric migration and interpret the ramified growth of electrodeposits with the model known as diffusion-limited aggregation [7]. Although thin cell geometry has been applied previously, the thickness of the electrolyte film still reaches several tens of micrometers [35]. Clearly, buoyancy convection can indeed be weakened in a thin cell deposition system, because the strength of convection is proportional to the quartic power of cell thickness [36]. However, electroconvection [27,30,33,34,37–40], an ignored ingredient in early studies of electrodeposition, remains an important factor in controlling the deposit morphology [33]. Is it possible to suppress the convective disturbance (including electroconvection) further in an electrodeposition system and make it really diffusion limited? Recently, we introduced a method to eliminate convection in electrodeposition [32,41]. By using the effect of segregation in solidifying an electrolyte solution at low temperature, an ultrathin layer of concentrated electrolyte can be generated between the ice of the electrolyte (solid) and the glass plate when equilibrium is established. The thickness of the ultrathin electrolyte layer depends on the initial concentration of electrolyte and temperature, and can be controlled to a few hundreds of nanometers. When the electrodeposition experiment is carried out in this ultrathin electrolyte layer, convective noise (i.e., random disturbance induced by convection) is expected to be suppressed significantly, and very regular metal branches with low branching rate are generated.

On the other hand, it has been shown in computer simulations that the branches of electrodeposits tend to be much straighter when a strong electric field is applied [42]. The mass transport in electrodeposition depends on both the concentration gradient (diffusion) and the strength of the local electric field (electromigration). It is suggested that the deposit morphology is determined by the competition of ion diffusion and ion electromigration. When the role of electromigration becomes more significant, the deposit morphology changes from a ramified, fractal-like pattern to straight filaments [42]. Therefore, we should identify the role of the electric field in the interfacial growth before we can draw conclusions about the physical origin for the formation of smooth electrodeposit branches in an ultrathin film system [32,41]. It is interesting to pinpoint the morphology of metal deposits in the ultrathin film system in the case without an external electric field. To reach this goal, we designed an electroless, ultrathin deposition system.

In this paper we report a self-organized electroless deposition of copper in an ultrathin layer of $CuSO_4$ electrolyte. The thickness of the electrolyte film is controlled by both the initial electrolyte concentration and temperature, and may reach just a few hundreds of nanometers. Experiments show that microscopically the branching rate of the copper deposits decreases significantly, and the deposits form an array of smooth, polycrystalline filaments. In this nearly ideal diffusion-limited system, we suggest that restriction of the thickness of electrolyte film is responsible for the suppression of the branching rate of the copper deposit. The ramified, fractal-like pattern seems not necessarily to be a characteristic feature of diffusion-limited aggregation.

II. EXPERIMENTAL SETUP AND RESULTS

The cell for electroless deposition consists of two cleaned glass plates, separated 100 μm by spacers, and a slice of zinc

*Author to whom correspondence should be addressed. Email address: muwang@nju.edu.cn

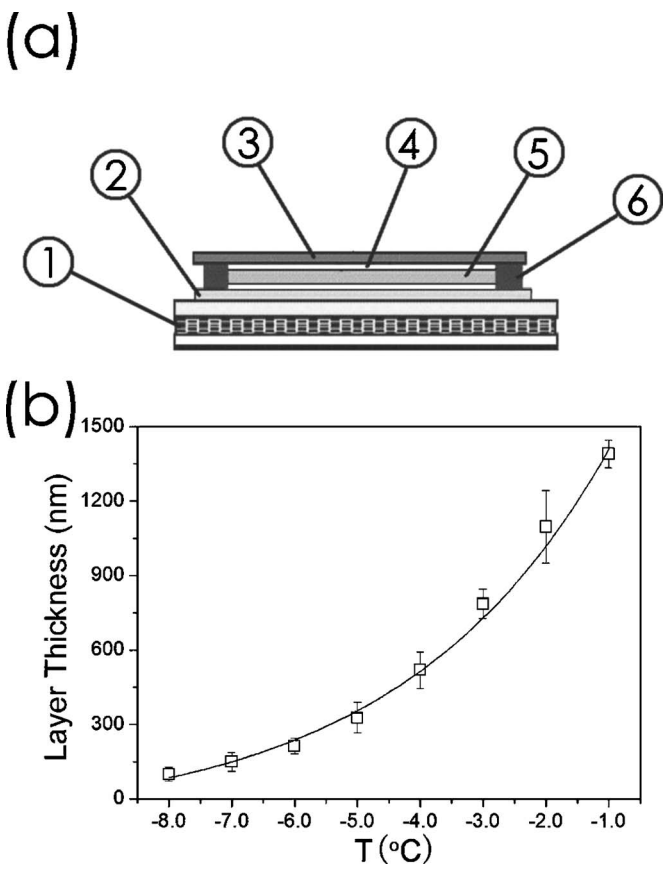

FIG. 1. (a) The kernel part of the setup for electroless deposition of copper. (1) Peltier element used for solidifying the electrolyte and control temperature; (2) bottom glass plate of the deposition cell; (3) top glass plate of the deposition cell; (4) ultrathin electrolyte layer trapped between the ice of electrolyte and the glass substrate due to the segregation effect; (5) ice of electrolyte; (6) zinc (or copper) foil slice. (b) Thickness of the ultrathin electrolyte layer as a function of temperature. The initial concentration of the electrolyte before solidification is 0.05*M*.

metal foil (99.9%, Goodfellow). The electrolyte solution was prepared using analytical reagent $CuSO_4$, and deionized, ultrapure water (electric resistivity 18.2 MΩ cm). The concentration of the prepared solution is 0.05*M*. A thermostat and a Peltier element are used to decrease the temperature of the cell and to solidify the electrolyte. Details of the temperature control in this experiment are the same as reported before [41], and the kernel part of the experimental setup is shown in Fig. 1(a). During solidification, $CuSO_4$ is partially expelled from the ice of the electrolyte due to the segregation effect [36,43–46]. This process continues until equilibrium is reached. Meanwhile an ultrathin layer of concentrated $CuSO_4$ electrolyte is trapped between the ice of the electrolyte and the glass plate of the cell, where electroless deposition will be carried out.

We expect that the electrolyte concentration in the trapped layer is the saturated concentration at the specific temperature. This is because once the concentration becomes higher than the saturation concentration at that temperature, supersaturation for crystallization is established, and salt crystals ($CuSO_4$ in our case) are nucleated and grow, until the equilibrium saturated concentration is reached. To determine the thickness of the trapped ultrathin layer of electrolyte, we first measure the electric conductivity of the saturated electrolyte solution of $CuSO_4$ at each different temperature. Thereafter, the electrolyte solution (0.05*M*) is solidified in the cell at a certain temperature. (For the purpose of determining the thickness of the trapped electrolyte layer, we do not use zinc foil in the cell. Instead, two parallel slices of copper foils with thickness of 0.1 mm are used as spacers.) We then measure the electric resistance across the cell between the copper foils. Since the width of the cell and the separation of the copper foils are fixed, and the electric conductivity of the saturated electrolyte is determined in advance, from the measured electric resistance we can easily get the thickness of the electrolyte film. The thickness of the trapped electrolyte film as a function of temperature is plotted in Fig. 1(b). This result depends on the initial concentration of the electrolyte. We should point out that the thickness of the trapped ultrathin layer is obtained under the assumption that the electrolyte film is homogeneous in thickness over the whole cell.

To investigate the morphology of the copper deposit without an external electric field, a zinc foil is used to replace one of the copper spacers. As soon as the zinc foil contacts the electrolyte, a replacement reaction takes place, and aggregates of copper crystallites are formed. The copper aggregate branches initiate from the zinc foil and invade the aqueous electrolyte film. Since no external electric voltage or current is applied, there should be no macroscopic electric migration in the system. The deposition process is observed *in situ* with a research optical microscope (Leitz Orthoplan-pol). The detail morphology and the structure of the copper deposit are further analyzed by a field-emission scanning electron microscope (LEO 1530VP) and a transmission electron microscope (Philips TECNAI F20).

In the beginning of the experiment, solidification of the electrolyte has not yet completed, and the electrolyte solution film is thick. Meanwhile, the deposit branches are ramified, and the surface of the deposit is very rough, as illustrated in the upper left part of Fig. 2. As the temperature drops, the thickness of the electrolyte film becomes thinner quickly. The rapid decrease of temperature is realized by adjusting the voltage applied on the Peltier element. Once the deposition takes place in the ultrathin electrolyte film trapped between the ice and the glass plate, the deposit morphology changes significantly. As illustrated in the lower right part of Fig. 2, unlike the very rough, coral-like branches, here the deposit becomes nearly two dimensional. Yet the tip-splitting rate remains high. In the following process, if temperature is not further decreased, the deposit will keep this fractal-like morphology. If, however, the temperature is decreased further, the density and the branching rate of the deposit will be changed accordingly. Figure 3 shows the deposit morphology at the region where temperature is abruptly decreased. In the upper left part of Fig. 3(a), the interbranch separation is larger than that shown in the lower right part. The detailed morphology of the transition region is shown in Fig. 3(b), and the difference of the two morphologies is clear. The deposit morphology developed at different temperatures is investigated. Figure 4(a) shows the copper branches achieved at −0.14 °C, where the branches are very ramified and

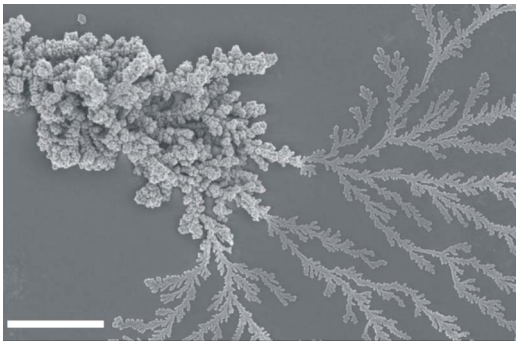

FIG. 2. (Color online) The deposit morphology of copper in the early stage of solidification of the electrolyte solution when the thickness of the electrolyte varies with time. The upper left part shows the deposit when the electrolyte solution film remains thick. Here the deposit branches are ramified and coral-like. As temperature drops, the electrolyte starts to solidify, and the aqueous layer trapped between the ice of the electrolyte and the glass plate becomes thinner and thinner. The lower right part shows the deposit branches developing in the trapped electrolyte film, where the copper deposits stick on the substrate surface. Yet at this stage the tip-splitting rate remains high. The scale bar represents 9 μm.

fractal-like. Figures 4(b) and 4(c) show the copper branches achieved at −2 and −8 °C, respectively. In Fig. 4(c) the deposit branches are much more space filling, forming a more compact fingering pattern instead of the dense branching morphology illustrated in Fig. 4(b). The branching rate of the deposits becomes much lower in Fig. 4(c) compared with that shown in Figs. 4(a) and 4(b). The screening effect is clear in Fig. 4, indicating that the diffusion field still plays a role. The structure of the copper deposit branches is determined with transmission electron microscopy (TEM) by carefully transferring the copper branches from the glass substrate to the TEM sample holder. The electron micrograph and the corresponding diffraction pattern are shown in Fig. 5. It is clear that the copper deposit is polycrystalline, and the size of the copper crystallites is of the order of 10 nm.

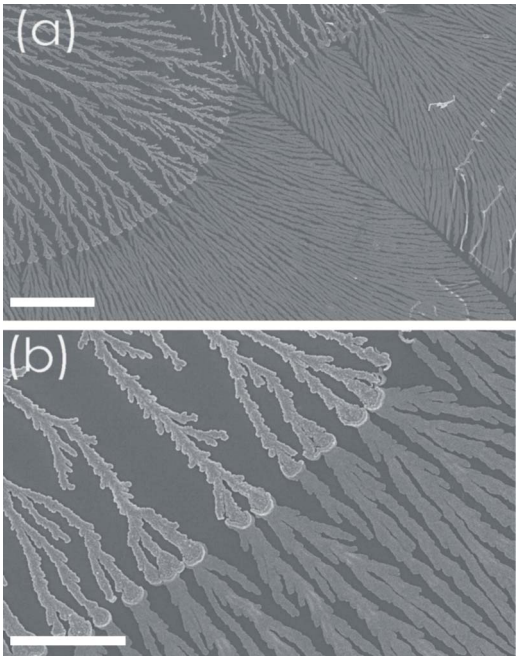

FIG. 3. (Color online) The deposit morphology of copper taken at the place where temperature (hence the thickness of the electrolyte) is changed abruptly. The density of the branch and branching rate of the deposits vary accordingly. The contrast of the branches in these two parts [as shown clearly in (b)] implies that the thickness of the copper deposit also changes. The branches with brighter contrast [upper left part of (b)] are thicker. The bar represents 20 μm in (a) and 6 μm in (b).

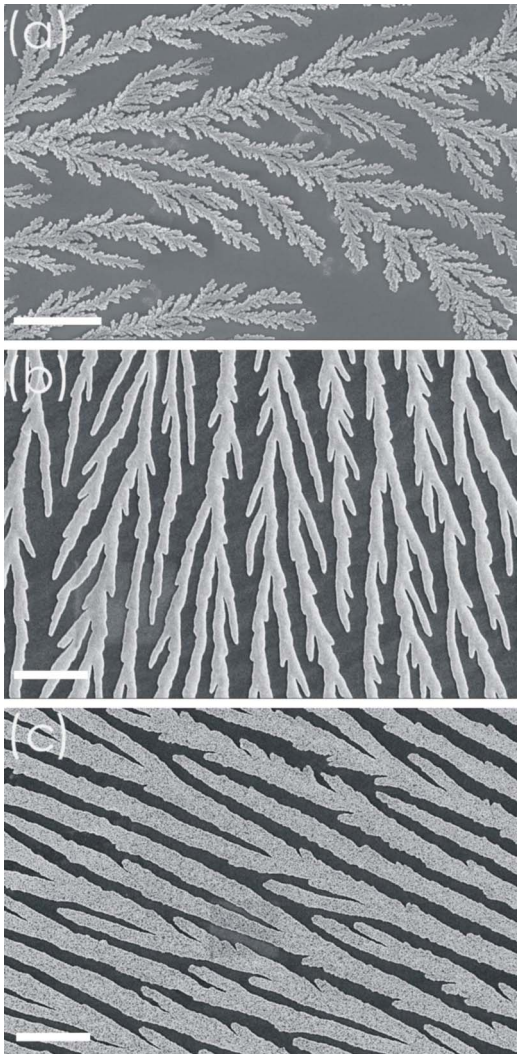

FIG. 4. (Color online) The deposit morphology of copper obtained at different temperatures. (a) shows the branches obtained at −0.14 °C, which remain fractal-like; (b) shows the deposit branches obtained at −2 °C, and (c) shows the deposit branches obtained at −8 °C. The scale bar in all these pictures represents 5 μm.

III. DISCUSSION

The copper branches generated in this experimental system are unique for two reasons. One is that we create an ultrathin electroless deposition system, where convection is expected to be significantly suppressed. It is generally accepted that the formation of ramified fractal-like branches is

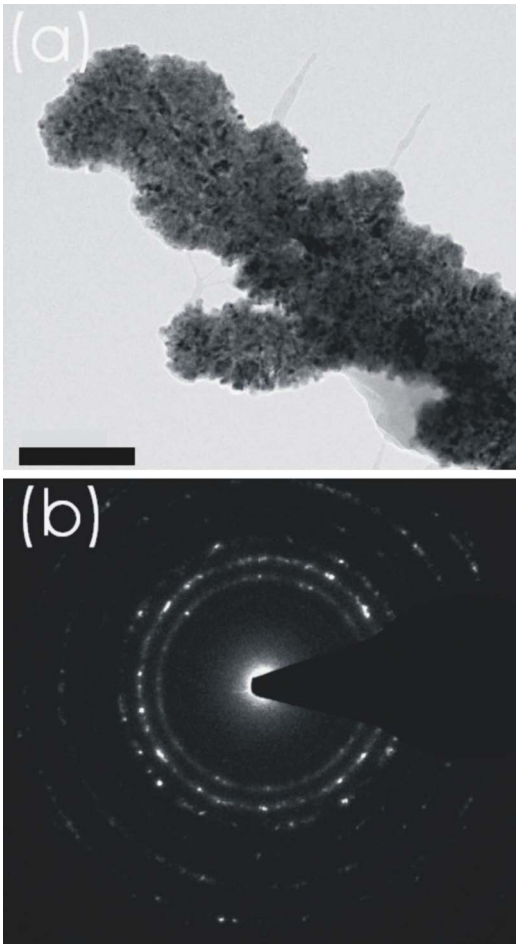

FIG. 5. (Color online) TEM pictures of the copper deposits. (a) shows the diffraction contrast image of a deposit branch. (b) shows the electron diffraction of the branch. It is clear that the deposit branch is polycrystalline. The bar represents 200 nm.

the characteristic feature of a diffusion-limited system when the role of surface tension is not significant [12,25–30]. As illustrated in Fig. 1, by solidifying the electrolyte, the typical thickness of the trapped electrolyte layer is a few hundreds of nanometers. In particular, by decreasing temperature by about 8 °C, the thickness of the electrolyte layer can be decreased by nearly ten times. We expect that both buoyancy convection [20,37,47] and electroconvection [27,30,33,34,37–40] are greatly reduced in such an ultrathin electrolyte layer, whereas convective disturbance is usually believed to contribute to tip splitting and formation of dense branching morphology. The second reason is that there is no external macroscopic electric field applied to our system, and the mass transfer is mostly contributed by diffusion, i.e., this growth system is exactly diffusion limited. According to our previous experiments of electrodeposition with $CuSO_4$ solution [41], changing the temperature from 30 to −5 °C (supercooling the electrolyte) or changing concentration from 0.008*M* to 0.8*M* does not significantly change the microscopic morphology of the deposit. We therefore suggest that the generation of smoother deposit branches and suppression of the tip-splitting rate should be caused by the decrease of the thickness of the electrolyte film. Physically this might imply that the reduction of convective disturbance in our ultrathin deposition system is responsible for the generation of a less random, more ordered morphology.

As indicated in Fig. 4(c), it is interesting to notice that in this noise-reduced diffusion-limited system, the deposit branches tend to be space filling. One may also find that some filaments have a nearly parabolic tip, and some tips can be stabilized for a distance as long as more than ten times the width of the filament. This is an interesting feature since the deposit branches are polycrystalline, and the crystallographic orientation of each crystallite is random [see the diffraction pattern in Fig. 5(b)]. In directional solidification (crystallization), the solid can be single crystalline and stable parabolic tips of the needlelike crystals are often observed when the supercooling has been sufficiently large [48]. According to the principle of microsolubility [6,49,50], when anisotropy exists in surface tension, the needle tip will remain the coldest point at an appropriate temperature field and will be stabilized against external disturbance. For the case of solidification of a single crystal from the melt, both interfacial tension and anisotropy in the interfacial tension are well defined. For the replacement reaction shown in this paper, however, the deposition is essentially an aggregation process of nanocrystallites. For such a granular material, it seems difficult to define an interfacial tension. At least, anisotropy of interfacial tension, due to the polycrystalline feature of the deposit, should vanish. Therefore it is interesting to note that some stable parabolic tips are still observable. One possible explanation is that there might be an effective surface tension in aggregating nanocrystallites, which prevents random tip splitting as usually seen in diffusion-limited aggregation.

For ramified growth where nucleation plays an important role, we once proposed a model known as "nucleation-limited aggregation," in which nucleation, instead of diffusion, controls the interfacial growth [51]. A similar idea was proposed by Fleury *et al.* in electrochemical deposition [12]. Once a crystallite is nucleated on the interface of the aggregate, the local concentration field is disturbed. Such a disturbance may act as a source to stimulate nucleation of the next generation of crystallites. Via such an avalanchelike nucleation process the metallic deposit is generated. For a thick electrolyte film, the impact of sudden nucleation of the copper nanocrystallite may stimulate further nucleation in an essentially three-dimensional space. Therefore a ramified metal "coral" like that shown in the upper left part of Fig. 2 is formed. When the thickness of the electrolyte solution is greatly reduced, the impact region of nucleation of the nanocrystallites is limited to the immediate neighborhood of the tip in two dimensions. An especially interesting scenario is that the density of the deposit branches is high. Due to the competition for nutrient supply in the diffusion field, adjacent deposit filaments will evidently confine each other when their separation is less than the thickness of the concentration boundary layer, bearing in mind that tip splitting occurs when the off-axis nucleation rate becomes as important as that along the axis of the filament. Yet in the case that the growing tips of the filaments are close to each other, the off-axis nucleation is restricted by the adjacent filament. Therefore, confinement of the neighboring branches, which is essentially a diffusion-limited effect, decreases the prob-

ability of tip splitting. In other words, the confinement of the adjacent filaments prohibits frequent nucleation in a direction not along the already existing deposit filaments, and eventually a two-dimensional array with low tip-splitting rate is formed. Such a process, although it takes place in a diffusion field, is different from conventional diffusion-limited aggregation [7] because interaction between neighboring tips (competition for nutrient supply) becomes very important in the interfacial kinetics.

To summarize, we report here a self-organized electroless deposition of copper in an ultrathin layer of $CuSO_4$ electrolyte. Microscopically the branching rate of the copper deposit is significantly decreased, forming an array of smooth, yet polycrystalline, copper filaments. Compared with conventional electrodeposition, no macroscopic electric field is applied and the thickness of the aqueous electrolyte layer is greatly reduced. This nearly ideal diffusion-controlled system and the growth behavior therein provide interesting information to understand pattern formation.

ACKNOWLEDGMENTS

The authors acknowledge the financial support of the Ministry of Science and Technology of China (Grant No. G2004CB619005) and the National Natural Science Foundation of China (Grant No. 10374043 and Grant No. 10021001). Discussions with V. Fleury, J. M. Liu, and Y. Q. Ma are also acknowledged.

[1] B. B. Mandelbrot, *The Fractal Geometry of Nature* (Freeman, San Francisco, 1982).
[2] T. Vicsek, *Fractal Growth Phenomena*, 2nd ed. (World Scientific, Singapore, 1992).
[3] *On Growth and Form*, edited by G. Stanley and N. Ostrowsky, NATO Advanced Studies Institute, Series B: Physics (Kluwer, Boston, 1986), Vol. 100.
[4] L. Kadanoff, J. Stat. Phys. **39**, 267 (1985).
[5] R. M. Brady and R. C. Ball, Nature (London) **309**, 225 (1984).
[6] E. Ben-Jacob and P. Garik, Nature (London) **343**, 523 (1990).
[7] T. A. Witten and L. M. Sander, Phys. Rev. Lett. **47**, 1400 (1981); Phys. Rev. B **27**, 5686 (1983).
[8] M. Q. Lopez-Salvans, J. Casademunt, G. Iori, and F. Sagues, Physica D **164**, 127 (2002).
[9] O. Younes, L. Zeiri, S. Efrima, and M. Deutsch, Langmuir **13**, 1767 (1997).
[10] M. Q. Lopez-Salvans, F. Sagues, J. Claret, and J. Bassas, Phys. Rev. E **56**, 6869 (1997).
[11] F. Texier, L. Servant, J. L. Bruneel, and F. Argoul, J. Electroanal. Chem. **446**, 189 (1998).
[12] V. Fleury, Nature (London) **390**, 145 (1997).
[13] D. P. Barkey, D. Watt, Z. Liu, and S. Raber, J. Electrochem. Soc. **141**, 1206 (1994).
[14] J. R. Melrose, D. B. Hibbert, and R. C. Ball, Phys. Rev. Lett. **65**, 3009 (1990).
[15] O. Zik and E. Moses, Phys. Rev. E **53**, 1760 (1996).
[16] S. N. Atchison, R. P. Burford, C. P. Whitby, and D. B. Hibbert, J. Electroanal. Chem. **399**, 71 (1995).
[17] V. Fleury, W. A. Watters, L. Allam, and T. Devers, Nature (London) **416**, 716 (2002).
[18] M. A. Pasquale, D. P. Barkley, and A. J. Arvia, J. Electrochem. Soc. **152**, C149 (2005).
[19] K. Fukami, S. Nakanishi, S. Sakai, and Y. Nakato, Chem. Lett. **32**, 532 (2003).
[20] M. Rosso, E. Chassaing, and J.-N. Chazalviel, Phys. Rev. E **59**, 3135 (1999).
[21] N. D. Koshel, Russ. J. Electrochem. **33**, 825 (1997).
[22] J. Elezgaray, C. Leger, and F. Argoul, Phys. Rev. Lett. **84**, 3129 (2000).
[23] M. Z. Zhang, Y. Wang, G. W. Yu, M. Wang, R. W. Peng, Y. Y. Weng, and N. B. Ming, J. Phys.: Condens. Matter **16**, 695 (2004).
[24] G. Marshall, F. V. Molina, and A. Soba, Electrochim. Acta **50**, 3436 (2005).
[25] M. Wang, X. Y. Liu, C. S. Strom, P. Bennema, W. van Enckevort, and N. B. Ming, Phys. Rev. Lett. **80**, 3089 (1998).
[26] K. K. Nanda and S. N. Sahu, Europhys. Lett. **60**, 397 (2002).
[27] G. Gonzalez, G. Marshall, F. V. Molina, S. Dengra, and M. Rosso, J. Electrochem. Soc. **148**, C479 (2001).
[28] F. Sagues, M. Q. Lopez-Salvans, and J. Claret, Phys. Rep. **337**, 97 (2000).
[29] C. Leger, F. Argoul, and M. Z. Bazant, J. Phys. Chem. B **103**, 5841 (1999).
[30] F. Argoul, A. Arneodo, J. Elezgaray, and A. Kuhn, Fractals **5**, 75 (1997).
[31] M. Q. López-Salvans, P. P. Trigueros, S. Vallmitjana, J. Claret, and F. Sagués, Phys. Rev. Lett. **76**, 4062 (1996); **77**, 4279 (1996).
[32] M. Wang, S. Zhong, X. B. Yin, J. M. Zhu, R. W. Peng, Y. Wang, K. Q. Zhang, and N. B. Ming, Phys. Rev. Lett. **86**, 3827 (2001).
[33] M. Wang, W. J. P. van Enckevort, N. B. Ming, and P. Bennema, Nature (London) **367**, 438 (1994).
[34] V. Fleury, J.-N. Chazalviel, M. Rosso, and B. Sapoval, J. Electroanal. Chem. Interfacial Electrochem. **290**, 249 (1990).
[35] J. M. Huth, H. L. Swinney, W. D. McCormick, A. Kuhn, and F. Argoul, Phys. Rev. E **51**, 3444 (1995).
[36] F. Rosenberger, *Fundamentals of Crystal Growth* (Springer-Verlag, Berlin, 1979).
[37] G. Marshall, P. Mocskos, H. L. Swinney, and J. M. Huth, Phys. Rev. E **59**, 2157 (1999).
[38] K. Q. Zhang, M. Wang, S. Zhong, G. X. Chen, and N. B. Ming, Phys. Rev. E **61**, 5512 (2000).
[39] J. R. deBruyn, Phys. Rev. E **56**, 3326 (1997).
[40] K. Q. Zhang, M. Wang, R. W. Peng, Y. M. Xiao, and N. B. Ming, Phys. Lett. A **278**, 286 (2001).
[41] S. Zhong, Y. Wang, M. Wang, M. Z. Zhang, X. B. Yin, R. W. Peng, and N. B. Ming, Phys. Rev. E **67**, 061601 (2003).
[42] J. Erlebacher, P. C. Searson, and K. Sieradzki, Phys. Rev. Lett. **71**, 3311 (1993).
[43] A. A. Chernov, *Modern Crystallography III: Crystal Growth* (Springer-Verlag, Berlin, 1984).

[44] N.-B. Ming, *Fundamentals of Crystal Growth Physics* (Shanghai Science and Technology, Shanghai, 1982).
[45] W. Kurz and D. J. Fisher, *Fundamentals of Solidification*, 4th ed. (Trans Tech Publications, Zurich, Switzerland, 1998).
[46] A. Pimpinelli and J. Villain, *Physics of Crystal Growth* (Cambridge University Press, Cambridge, U.K., 1998).
[47] G. Gonzalez, G. Marshall, F. Molina, and S. Dengra, Phys. Rev. E **65**, 051607 (2002).
[48] X. Tong, C. Beckermann, A. Karma, and Q. Li, Phys. Rev. E **63**, 061601 (2001).
[49] E. Ben-Jacob, Nigel Goldenfeld, B. G. Kotliar, and J. S. Langer, Phys. Rev. Lett. **53**, 2110 (1984).
[50] A. Karma and W. J. Rappel, Phys. Rev. Lett. **77**, 4050 (1996).
[51] N. B. Ming, M. Wang, and R. W. Peng, Phys. Rev. E **48**, 621 (1993).